Broken-Symmetry Density Functional Theory Analysis of the Ω Intermediate in Radical *S*-Adenosyl-L-Methionine Enzymes: Evidence for a Near-Attack Conformer over an Organometallic Species

Patrick H. Donnan and Steven O. Mansoorabadi*

Department of Chemistry and Biochemistry, Auburn University, 179 Chemistry Building, Auburn, Alabama 36849, United States

ABSTRACT: Radical *S*-adenosyl-L-methionine (SAM) enzymes are found in all domains of life and catalyze a wide range of biochemical reactions. Recently, an organometallic intermediate, Ω, has been experimentally implicated in the 5′-deoxyadenosyl radical generation mechanism of the radical SAM superfamily. In this work, we employ broken-symmetry density functional theory (BS-DFT) to evaluate several structural models of Ω. The results show that the calculated hyperfine coupling constants (HFCCs) for the proposed organometallic structure of Ω are inconsistent with experiment. In contrast, a near-attack conformer of SAM bound to the catalytic [4Fe–4S] cluster, in which the distance between the unique iron and SAM sulfur is ~3 Å, yields HFCCs that are all within 1 MHz of the experimental values. These results clarify the structure of the ubiquitous Ω intermediate and suggest a paradigm shift reversal regarding the mechanism of SAM cleavage by members of the radical SAM superfamily.

Utilizing *S*-adenosyl-L-methionine (SAM) and iron-sulfur clusters, radical SAM (RS) enzymes are one of nature's most preeminent ways of generating radicals for use in biological catalysis. First identified as an enzyme superfamily in 2001,[1] RS enzymes have since been found in every domain of life and shown to catalyze an ever-increasing set of chemical reactions, from unactivated C-H bond functionalization to complex skeletal rearrangements.[2] Central to canonical RS chemistry is the radical generation mechanism: SAM bound to a reduced [4Fe–4S]$^{1+}$ cluster is reductively cleaved to form the 5′-deoxyadenosyl radical (5′-dAdo•) and methionine bound to an oxidized [4Fe–4S]$^{2+}$ cluster (Figure 1). It was previously thought that the 5′-dAdo• was formed directly through inner sphere electron transfer within the SAM-[4Fe–4S]$^{1+}$ complex. However, recent electron paramagnetic resonance (EPR) and electron-nuclear double resonance (ENDOR) spectroscopic investigations have identified a transient intermediate common to many enzymes in the RS superfamily. Initially found in pyruvate formate-lyase activating enzyme (PFL-AE), the so-called Ω intermediate (Figure 1) was then found in many other RS enzymes, including lysine-2,3-aminomutase (LAM), spore photoproduct lyase (SPL), and the [FeFe]-hydrogenase maturation protein HydG.[3-5] A similar intermediate was later found in the non-canonical RS enzyme Dph2 involved in diphthamide biosynthesis.[6]

The detection of Ω, in tandem with the discovery that SAM can be photolyzed to generate 5′-dAdo• in the absence of substrate, has influenced a growing number of recent experiments, including studies of ChuW, SuiB, ArsS, HydG, and spore photoproduct lyase.[7,8] Fundamental studies of RS enzymes have continued to provide evidence of or support for Ω.[7,9] Synthetic models of the organometallic Ω structure have been prepared and demonstrated Fe-C bond homolysis reactivity.[10] Computational investigations of Ω, on the other hand, have been sparse. A quantum mechanics/molecular mechanics (QM/MM) investigation of the transition states between a SAM-bound [4Fe–4S]$^{1+}$ cluster and Ω has been conducted, and it was suggested that organometallic Ω could be a possible shunt product of PFL-AE due its large, rate-limiting transition state (>16.7 kcal/ mol).[11]

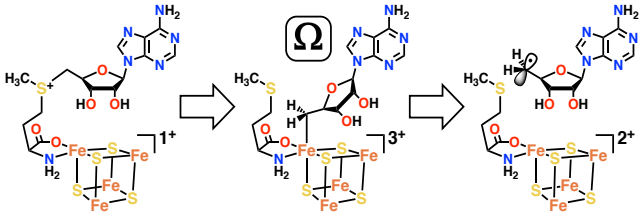

Figure 1. Reductive SAM cleavage reaction catalyzed by members of the radical SAM superfamily. The proposed organometallic structure of the Ω intermediate is shown.

Yet, the rates of Ω formation and decay in PFL-AE were shown to be catalytically competent, and its pervasiveness among characterized RS enzymes indicates that it is not a shunt product.[4] Turning to the initial experiments used to determine the structure of Ω may help provide a bridge between the QM/MM derived reaction energetics indicating a possible shunt product and experimental observations of catalytic competency. Well-defined *g*-values, and, more importantly, hyperfine coupling constants (HFCCs) were determined for Ω, and these values can be compared with theoretical estimates from structural models to provide evidence for or against Ω as an organometallic species.

Table 1. Calculated and Experimental Hyperfine Coupling Constants (in MHz) for structural models of Ω.[a]

Structural Model	5′-^{13}C	4′-^{13}C	methyl-^{13}C	5′-C–^{1}H[b]	Reference
Experiment	9.4	~0.5	~0.5	7-8	3,4
Proposed Organometallic Structure	140.4 ± 12.6	4.4 ± 2.9	0.03 ± 0.01	11.7 ± 14.1	This work
Crystallographic SAM-bound Cluster	1.5 ± 1.4	0.1 ± 0.1	0.9 ± 0.4[c]	0.9 ± 1.0	This work
SAM-NAC Structure (3.0 Å Fe-S Distance)	8.8 ± 1.0	0.6 ± 0.05	1.3 ± 0.8[c]	6.3 ± 0.2	This work

[a]The average and standard deviation of the absolute value of HFCCs from $m_S = +1/2$ BS states are reported.

[b]The larger of the two 5′-C–^{1}H HFCCs is reported.

[c]Due to close proximity to both apical Fe atoms, this methyl group is treated as a bridging ligand during spin projection.

Here, we report broken-symmetry density functional theory (BS-DFT) calculations of different models of the Ω intermediate to obtain 5′-^{13}C, 4′-^{13}C, methyl-^{13}C, and 5′-C–^{1}H HFCCs for comparison with experiment. BS-DFT has been a powerful tool in studying the electronic structure of antiferromagnetically coupled metal centers in biological systems, including iron- sulfur clusters, the oxygen-evolving complex of photosystem II, and the FeMo-cofactor of nitrogenase (including predicting the identity of ligand X ahead of experiments).[12-14] Utilizing the fundamental BS-DFT methodology established by Noodleman and co-workers, combined with the more recent HFCC calculation approach developed by Pantazis, Neese, and co-workers, we carried out geometry optimization and single point energy calculations of the proposed organometallic structure of Ω and of SAM bound to a [4Fe–4S]$^{1+}$ cluster in the conformation observed in the crystal structure of PFL-AE.[15-18] Since it is unknown which low-spin BS state/valence isomer corresponds best to the physical state of Ω in the active site of RS enzymes, we report an average value for the spin-projected HFCCs of the BS valence isomers with m_S = +1/2 (see SI for full computational details, including a discussion of BS states and spin projection factors).

Calculations of the organometallic species revealed HFCCs for 5′-^{13}C and 4′-^{13}C that were an order of magnitude too large to be consistent with the experimentally observed values (Table 1). Similarly, the calculated 5′-C–^{1}H HFCC is larger than the experimental value (Table 1). In contrast, the corresponding HFCCs of the geometry-optimized, crystallographic SAM-bound [4Fe–4S]$^{1+}$ cluster are 5-8 times too small to reproduce the experimental values. Because neither the proposed organometallic structure nor the crystallographic SAM-bound cluster have HFCCs consistent with experiment, we then calculated structures of SAM near-attack conformers (SAM-NACs) by constraining the distance between the unique iron of the cluster and the sulfur atom of SAM.[19]

In the optimized crystallographic geometry this distance is 3.53 Å; distance constraints of 3.2 Å, 3.0 Å, 2.8 Å, and 2.6 Å were employed for the NAC calculations. When analyzed after single point energy calculations on geometries optimized at each fixed distance, the NACs gave 5′-^{13}C, 4′-^{13}C, and 5′-C–^{1}H hyperfine couplings smaller than the organometallic structure but larger than the crystallographic SAM-bound cluster. The experimentally determined HFCCs lie within the range of these calculated values, which vary exponentially with the Fe-S distance (Figure 2). For example, the 5′-^{13}C HFCC increases from 4.5 MHz at 3.2 Å to 13.7 MHz at 2.8 Å, bracketing the experimental value of 9.4 MHz.

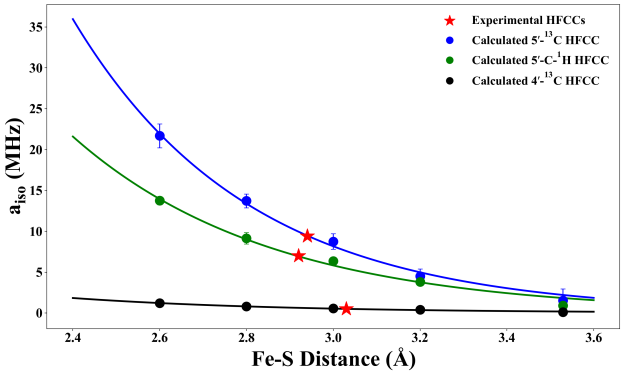

Figure 2. Calculated ^{13}C and ^{1}H isotropic hyperfine coupling constants (HFCCs) for SAM near-attack conformer (SAM-NAC) geometries with fixed unique iron–SAM sulfur distances. Calculated values are averaged over all BS valence isomers with m_S = +1/2 for each fixed distance with error bars showing the standard deviation. The average HFCCs for 5′-^{13}C (blue), 5′-C–^{1}H (green), and 4′-^{13}C (black) are shown as circles and best fit curves to a decaying exponential equation are shown as lines. The red stars indicate the experimentally determined HFCCs for each curve.

Assuming the experimentally detected species is a SAM-NAC, we can use the best fit curves for each HFCC to determine a unique iron–SAM sulfur distance that corresponds to the experimental values. For the 5′-^{13}C, 4′-^{13}C, and 5′-C–^{1}H HFCCs, the estimated Fe–S distance for Ω are self-consistent, ranging from 2.92 Å to 3.03 Å (Figure 2). Thus, of all the structural models considered, a SAM-NAC structure with an Fe-S distance of 3.0 Å most closely matches the experimental isotropic HFCCs of Ω (Table 1). Moreover, the calculated axial dipolar coupling for the 5′-^{13}C of this structure, $2T$ = 6.0 ± 0.6 MHz, also closely matches the experimental value of ~5.3 MHz, while the value for the organometallic model is again over an order of magnitude too large ($2T$ = 44.0 ± 8.8 MHz). The only calculated HFCC whose best fit curve did not predict an Fe-S bond distance of ~3 Å for Ω was for the methyl-^{13}C of SAM (Figure S2). However, this atom is unique in that it is approximately equidistant to each of the Fe atoms in the apical face of the cluster in the SAM-NAC structures (Table S1) and must therefore be treated similar to a bridging ligand during spin projection (see SI for details). Because the spin projection factors of the apical Fe atoms are opposite in sign, the net result is a cancellation effect that greatly diminishes the calculated methyl-^{13}C HFCC. This explains the unexpectedly small experimental methyl-^{13}C HFCC that was taken as evidence for 5′-C–S bond cleavage and the migration of the methionine side chain away from the cluster upon Ω formation.

The other experimental observation that was critical for the initial assignment of Ω as an organometallic species was the relatively large experimental 5′-^{13}C HFCC.[3] For this model, the 5′-C is alpha to the spin-bearing unique iron. Beta hyperfine interactions are also known to give rise to large HFCCs in organic radicals, depending on the dihedral angle of the relevant bond relative to the *p*-orbital of the spin-bearing carbon. Similarly, the large isotropic 5′-^{13}C HFCC of the SAM-NAC structure can be rationalized as a beta hyperfine interaction/hyperconjugative effect arising from the alignment of the 5′-C–S bond of SAM with the *d*-orbital(s) of the adjacent unique iron. This gives rise to a more modest 5′-^{13}C HFCC in the SAM-NAC structure that is consistent with the experimental value for Ω, as opposed to the very large alpha coupling predicted to be observed with the organometallic structure.

In order to verify the energetic feasibility of the SAM-NAC structure, we examined the relative energy curves of the system as the distance between the unique iron and SAM sulfur is constrained (Figure 3). We found that as the distance is shortened from the optimized crystallographic distance of 3.53 Å down to the predicted distance of 3 Å, the energy increases by less than 3 kcal mol^{-1} for each low-spin BS valence isomer. As the Fe-S distance is decreased further from 3.0 Å to 2.8 Å, the change in energy is even smaller, less than 1 kcal mol^{-1}. This provides a low energy plateau in the potential energy surface and suggests there could be a local minimum within the region corresponding to the SAM-NAC structure of Ω that can be stabilized within the active site of RS enzymes.

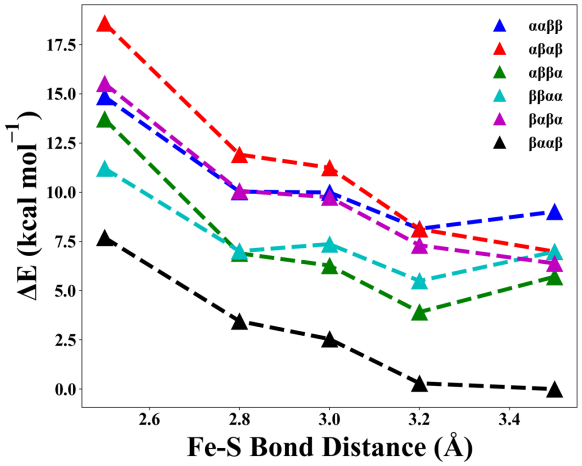

Figure 3. Relative energy curves for the broken-symmetry (BS) valence isomers of the SAM near-attack conformers (SAM-NACs) as a function of the unique iron–SAM sulfur distance.

Indeed, Rohac et al. recently provided compelling evidence for this by determining the structure of the RS enzyme HydE after its reaction was reductively triggered *in crystallo*.[20] Electron density within the active site was consistent with a 50-50 mixture of cleaved and uncleaved SAM.[20] Post-cleavage, the sulfur of the liberated methionine formed a 2.87 Å coordinate bond with the unique iron, while the Fe-S distance for the intact SAM-bound cluster was 3.08 Å, which is fully consistent with our predicted SAM-NAC structure of Ω. Moreover, no density was attributable to an organometallic structure containing a 5′-C–Fe bond or an altered methionine geometry.[20]

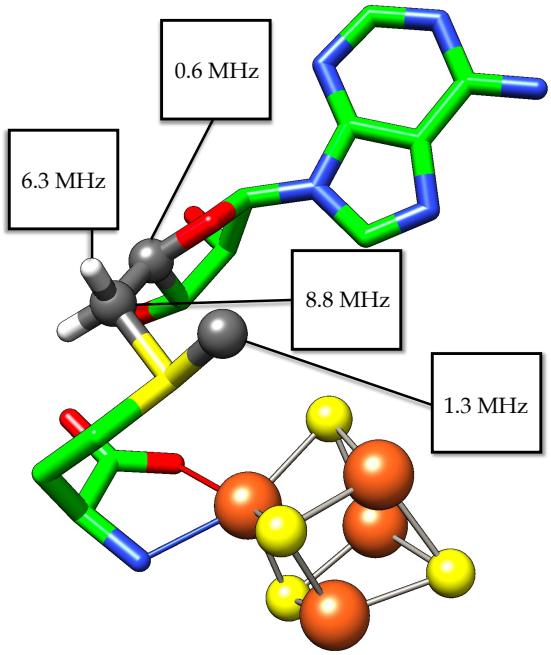

Figure 4. Proposed structure for the SAM near-attack conformer (SAM-NAC) structure of the Ω intermediate, with calculated HFCCs labeled. Hydrogens (except those on the 5′-C) and coordinated methanethiolate ligands used in the calculations are omitted for clarity.

Thus, we offer a new proposed structure for the Ω intermediate of RS catalysis: a SAM-NAC with an Fe–S bond distance of ~3 Å (Figure 4). Such a species is consistent with all known experimental and computational evidence and reconciles previous findings that an organometallic Ω is likely to be a shunt product while Ω itself is known to be catalytically competent. Our model of Ω as a SAM-NAC is consistent with the Frey catalytic model of 5′-dAdo• formation by RS enzymes and can be thought of as the structure along the reaction coordinate wherein the nonbonding electron pair of the sulfonium of SAM is brought in close proximity to the unique iron of the cluster.[21] Such a model also obviates the need for methionine gymnastics after SAM cleavage to allow 5′-dAdo• coupling to the [4Fe–4S]$^{2+}$ cluster and the requirement of having to pass through the same transition state twice to effect substrate hydrogen atom abstraction. Our reassignment of Ω as a NAC of SAM bound to the catalytic [4Fe–4S] cluster thus has significant implications for the radical generation mechanism of RS enzymes and should help guide future experimental and computational studies of this important enzyme superfamily.

ASSOCIATED CONTENT

Supporting Information

The Supporting Information is available free of charge on the ACS Publications website.

Computational details, a discussion of broken-symmetry DFT and spin projection, tabulated BS state energies, Mulliken spin populations, *J*-values, and spin projection factors, calculated hyperfine tensors for BS valence isomers, methyl-^{13}C HFCCs vs. unique Fe–SAM S distance plot, coordinates of all geometry optimized structures used in single point calculations, and supporting references. (PDF).

AUTHOR INFORMATION

Corresponding Author

Steven O. Mansoorabadi—Department of Chemistry and Biochemistry, Auburn University, 179 Chemistry Building, Auburn, Alabama 36849, United States; https://orcid.org/0000-0002-6369-3815; Email: som@auburn.edu

Author

Patrick H. Donnan—Department of Chemistry and Biochemistry, Auburn University, 179 Chemistry Building, Auburn, Alabama 36849, United States; https://orcid.org/0000-0002-8076-2683

Notes

The authors declare no competing financial interests.

ACKNOWLEDGMENT

P. H. D. was supported by a fellowship from the National Science Foundation (NSF) Established Program to Stimulate Competitive Research (EPSCoR) associated with NSF CAREER Award CHE-1555138 (from the Division of Chemistry) awarded to S. O. M. This work was supported by the U.S. Department of Energy (DOE), Office of Science, Basic Energy Sciences (BES) under DOE Early Career Award DE-SC0018043 and by a grant of high-performance computing resources and technical support from the Alabama Supercomputer Authority.

REFERENCES

(1) Sofia, H. J.; Chen, G.; Hetzler, B. G.; Reyes-Spindola, J. F.; Miller, N. E. Radical SAM, a novel protein superfamily linking unresolved steps in familiar biosynthetic pathways with radical mechanisms: functional characterization using new analysis and information visualization methods. *Nucleic Acids Res.* **2001**, *29* (5), 1097–1106.

(2) (a) Frey, P. A.; Hegeman, A. D.; Ruzicka, F. J.; The Radical SAM Superfamily. *Crit. Rev. Biochem. Mol. Bio.* **2008**, *43* (1), 63–88. (b) Broderick, J. B.; Duffus, B. R.; Duschene, K. S.; Shepard, E. M. Radical *S*-adenosylmethonine Enzymes. *Chem. Rev.* **2014**, *114* (8), 4220–4317. (c) Landgraf, B. J.; McCarthy, E. L.; Booker, S. J. Radical S-Adenosylmethionine Enzymes in Human Health and Disease. *Annu. Rev. Biochem.* **2016**, *85* (1), 485–514. (d) Bridwell-Rabb, J.; Grell, T. A. J.; Drennan, C. L. A Rich Man, Poor Man Story of *S*-Adenosylmethionine and Cobalamin Revisited. *Annu. Rev. Biochem.* **2018**, *87* (1), 555–584. (e) Nicolet, Y. Structure–Function relationships of radical SAM enzymes. *Nature Catalyis* **2020,** *3*, 337–350.

(3) Horitani, M.; Shisler, K.; Broderick, W. E.; Hutcheson, R. U.; Duschene, K. S.; Marts, A. R.; Hoffman, B. M.; Broderick, J. B. Radical SAM Catalysis via an organometallic intermediate with an Fe-[5′-C]-deoxyadenosyl bond. *Science* **2016**, *352* (6287), 822–825.

(4) Byer, A. S.; Yang, H.; McDaniel, E. C.; Kathiresan, V.; Impano, S.; Pagnier, A.; Watts, H.; Denler, C.; Vagstad, A. L.; Piel, J.; Duschene, K. S.; Shepard, E. M.; Shields, T. P.; Scott, L. G.; Lilla, E. A.; Yokoyama, K.; Broderick, W. E.; Hoffman, B. M.; Broderick, J. B. Paradigm Shift for Radical-*S*-Adenosyl-L-Methionine Reactions: The Organometallic Intermediate Ω is Central to Catalysis. *J. Am. Chem. Soc.* **2018**, *140* (28), 8634–8638.

(5) Broderick, W. E.; Hoffman, B. M.; Broderick, J. B. Mechanism of Radical Initiation in the Radical-*S*-Adenosyl-L-Methionine Superfamily. *Acc. Chem. Res.* **2018**, *51* (11), 2611–2619.

(6) Dong, M.; Kathiresan, V.; Fenwick, M. K.; Torelli, A. T.; Zhang, Y.; Caranto, J. D.; Dzikovski, B.; Sharma, A.; Lancaster, K. M.; Freed, J. H.; Ealick, S. E.; Hoffman, B. M.; Lin, H. Organometallic and radical intermediates reveal mechanism of diphthamide biosynthesis. *Science* **2018**, *359* (6381), 1247–1250.

(7) Yang, H.; McDaniel, E. C.; Impano, S.; Byer, A. S.; Jodts, R. J.; Yokoyama, K.; Broderick, W. E.; Broderick, J. B.; Hoffman, B. M. The Elusive 5′-Deoxyadenosine Radical: Captured and Characterized by Electron Paramagnetic Resonance and Electron Nuclear Double Resonance Spectroscopies. *J. Am. Chem. Soc.* **2019**, *41* (30), 12130–12146.

(8) (a) Liju, M. G.; Beattie, N. R.; Pritchett, C.; Lanzilotta, W. N. New Insight into the Mechanism of Anaerobic Heme Degradation. *Biochemistry* **2019**, *58* (46), 4641–4654. (b) Balo, A. R.; Caruso, A.; Tao, L.; Tantillo, D. J.; Seyedsayamdost, M. R.; Britt, D. R. Trapping a cross-linked lysine–tryptophan radical in the catalytic cycle of the radical SAM enzyme SuiB. *Proc. Natl. Acad. Sci. U.S.A.* **2021**, *118* (21), e2101571118. (c) Cheng, J.; Ji, W.; Ma, S.; Ji, X.; Deng, Z.; Ding, W.; Zhang, Q. Characterization and Mechanistic Study of the Radical SAM Enzyme ArsS Involved in Arsenosugar Biosynthesis. *Angew. Chem. Int. Ed.* **2021**, *60* (14), 7570–7575. (d) Impano, S.; Yang, H.; Shepard, E. M.; Swimley, R.; Pagnier, A.; Broderick, W. E.; Hoffman, B. M.; Broderick, J. B. S-Adenosyl-L-ethionine is a Catalytically Competent Analog of S-Adenosyl-L-methionine (SAM) in the Radical SAM Enzyme HydG. *Angew. Chem. Int. Ed.* **2021**, *60* (9), 4666–4672. (e) Pagnier, A.; Yang, H.; Jodts, R. J.; James, C. D.; Shepard, E. M.; Impano, S.; Broderick, W. E.; Hoffman, B. M.; Broderick, J. B. Radical SAM Enzyme Spore Photoproduct Lyase: Properties of the Ω Organometallic Intermediate and Identification of Stable Protein Radicals Formed during Substrate-Free Turnover. *J. Am. Chem. Soc.* **2020**, *142* (43), 18652–18660.

(9) (a) Miller, S. A.; Bandarian, V. Analysis of Electrochemical Properties of *S*-Adenosyl-L-methionine and Implications for Its Role in Radical SAM Enzymes. *J. Am. Chem. Soc.* **2019**, *141* (28) 11019–11026. (b) Yang, H.; Impano, S.; Shepard, E. M.; James, C. D.; Broderick, W. E.; Broderick, J. B.; Hoffman, B. M. Photoinduced Electron Transfer in a Radical SAM Enzyme Generates an *S*-Adenosylmethionine Derived Methyl Radical. *J. Am. Chem. Soc.* **2019**, *141* (40) 16117–16124. (c) Sayler, R. I.; Stich, T. A.; Joshi, S.; Cooper, N.; Shaw, J. T.; Begley, T. P.; Tantillo, D. J.; Britt, R. D. Trapping and Electron Paramagnetic Resonance Characterization of the 5′ dAdo• Radical in Radical *S*-Adenosyl Methionine Enzyme Reaction with a Non-Native Substrate. *ACS Cent. Sci.* **2019**, *5* (11), 1777–1785. (d) Impano, S.; Yang, H.; Jodts, R. J.; Pagnier, A.; Swimley, R.; McDaniel, E. C.; Shepard, E. M.; Broderick, W. E.; Broderick, J. B.; Hoffman, B. M. Active-Site Controlled, Jahn–Teller Enabled Regioselectivity in Reductive S–C Bond Cleavage of S-Adenosylmethionine in Radical SAM Enzymes. *J. Am. Chem. Soc.* **2021**, *143* (1), 335–348.

(10) (a) Ye, M.; Thompson, N. B.; Brown, A. C.; Suess, D. L. M. A Synthetic Model of Enzymatic $[Fe_4S_4]$–Alkyl Intermediates. *J. Am. Chem. Soc.* **2019**, *141* (34), 13330–13335. (b) Brown, A. C.; Suess, D. L. M. Reversible Formation of Alkyl Radicals at $[Fe_4S_4]$ Clusters and Its Implications for Selectivity in Radical SAM Enzymes. *J. Am. Chem. Soc.* **2020**, *142* (33), 14240–14248.

(11) Zhao, C.; Li, Y.; Wang, C.; Chen, H. Mechanistic Dichotomy in the Activation of SAM by Radical SAM Enzymes: QM/MM Modeling Deciphers the Determinant. *ACS Catal.* **2020**, *10*, 13245–13250.

(12) (a) Noodleman, L. A Model for the Spin States of High-Potential Iron-Sulfur $[Fe_4S_4]^{3+}$ Proteins. *Inorg. Chem.* **1988**, *27* (20), 3677– 3679. (b) Noodleman, L. Exchange Coupling and Resonance Delocalization in Reduced $[Fe_4S_4]^{+}$ and $[Fe_4S_4]^{+}$ Clusters. 2. A Generalized Nonlinear Model for Spin-State Energies and EPR and Hyperfine Properties. *Inorg. Chem.* **1991**, *30* (2), 256–264. (c) Torres, R. A.; Lovell, T.; Noodleman, L.; Case, D. A. Density Functional and Reduction Potential Calculations of Fe_4S_4 Clusters. *J. Am. Chem. Soc.* **2003**, *125* (7), 1923–1936. (d) Blachy, P. G.; Sandala, G. M.; Giammona, D. A.; Bashford, D.; McCammon, J. A.; Noodleman, L. Broken-Symmetry DFT Computations for the Reaction Pathway of IspH, an Iron–Sulfur Enzyme in Pathogenic Bacteria. *Inorg. Chem.* **2015**, *54* (13), 6439–6461.

(13) (a) Schinzel, S.; Schraut, J.; Arbuzniko, A. V.; Siegbahn, P. E. M.; Kaupp, M. Density Functional Calculations of ^{55}Mn, ^{14}N, and ^{13}C Electron Paramagnetic Resonance Parameters Support an Energetically Feasible Model System for the S_2 State of the Oxygen-Evolving Complex of Photosystem II. *Chem. Eur. J.* **2010**, *16* (34), 10424–10438. (b) Pantazis, D. A.; Ames, W.; Cox, N.; Lubitz, W.; Neese, F. Two Interconvertible Structures that Explain the Spectroscopic Properties of the Oxygen-Evolving Complex of Photosystem

II in the S_2 State. *Angew. Chem. Int. Ed.* **2012**, *51* (39), 9935–9940. (c) Beal., N. J.; Corry, T. A.; O'Malley, P. J. A Comparison of Experimental and Broken-Symmetry Density Functional Theory (BS-DFT) Calculated Electron Paramagnetic Resonance (EPR) Parameters for Intermediates Involved in the S_2 to S_3 State Transition of Nature's Oxygen Evolving Complex. *J. Phys. Chem. B* **2018**, *122* (4), 1394–1407. (d) Yang, K. R.; Lakshmi, K. V.; Brudvig, G. W.; Batista, V. S. Is Deprotonation of the Oxygen-Evolving Complex of Photosystem II during the $S_1 \rightarrow S_2$ Transition Suppressed by Proton Quantum Delocalization? *J. Am. Chem. Soc.* **2021**, *143* (22), 8324–8332.

(14) (a) Lovell, T.; Li, J. Lui, T.; Case, D. A.; Noodleman, L. FeMo Cofactor of Nitrogenase: A Density Functional Study of States M^N, M^{OX}, M^R, and M^I. *J. Am. Chem. Soc.* **2001**, *123* (49), 12393–12410. (b) Pelmenschikov, V.; Case, D. A.; Noodleman, L. Ligand-Bound *S* = ½ FeMo-Cofactor of Nitrogenase: Hyperfine Interaction Analysis and Implication for the Central Ligand X Identity. *Inorg. Chem.* **2008**, *47* (14), 6162–6172. (c) Benediktsson, B.; Bjornsson, R. QM/MM Study of the Nitrogenase MoFe Protein Resting State: Broken-Symmetry States, Protonation States, and QM Region Convergence in the FeMoco Active Site. *Inorg. Chem.* **2017**, *56* (21), 13417–13429. (d) Raugei, S.; Seefeldt, L. C; Hoffman, B. M. Critical computational analysis illuminates the reductive-elimination mechanism that activates nitrogenase for N_2 reduction. *Proc. Natl. Acad. Sci. U.S.A.* **2018**, *115* (45), E10521–E10530.

(15) Noodleman, L.; Peng, C. Y.; Case, D. A.; Mouesca, J.-M.; Orbital interaction, electron delocalization and spin coupling in iron-sulfur clusters. *Coord. Chem. Rev.* **1995**, *144,* 199–244.

(16) Pantazis, D. A.; Orio, M.; Petrenko, T.; Zein, S.; Bill, E.; Lubitz, W.; Messinger, J.; Neese, F. A New Quantum Chemical Approach to the Magnetic Properties of Oligonuclear Transition-Metal Complexes: Application to a Model for the Tetranuclear Manganese Cluster of Photosystem II. *Chem. Eur. J.* **2009**, *15* (20), 5108–5123.

(17) (a) Neese, F. The ORCA program system. *Wiley Interdiscip. Rev.: Comput. Mol. Sci.* **2012**, *2*, 73–78. (b) Neese, F. Software update: the ORCA program system, version 4.0. *Wiley Interdiscip. Rev.: Comput. Mol. Sci.* **2017**, *8*, e1327. (c) Perdew, J. P. Density-functional approximation for the correlation energy of the inhomogeneous electron gas. *Phys. Rev. B* **1986**, *33* (12), 8822–8824. (d) Becke, A. D. Density-functional exchange-energy approximation with correct asymptotic behavior. *Phys. Rev. A* **1988**, *38* (6), 3098–3100. (e) Staroverov, V. N.; Scuseria, G. E.; Tao, J.; Perdew, J. P. Comparative assessment of a new nonempirical density functional: Molecules and hydrogen-bonded complexes. *J. Chem. Phys.* **2003**, *119* (23), 12129. (f) Weigend, F.; Ahlrichs, R. Balanced basis sets of split valence, triple zeta valence and quadruple zeta valence quality for H to Rn: Design and assessment of accuracy. *Phys. Chem. Chem. Phys.* **2005**, *7* (18), 3297–3305. (g) Weigend, F. Accurate Coulomb-fitting basis sets for H to Rn. *Phys. Chem. Chem. Phys.* **2006**, *8* (9), 1057–1065. (h) Rega, N.; Cossi, M.; Barone, V. Development and validation of reliable quantum mechanical approaches for the study of free radicals in solution. *J. Chem. Phys.* **1996**, *105* (24), 11060. (i) Neese. F.; Prediction and interpretation of the ^{57}Fe isomer shift in Mössbauer spectra by density functional theory. *Inorg. Chim. Acta* **2002**, *337*, 181–192. (j) Neese, F.; Wennmoh, F.; Hansen, A.; Becker, U. Efficient, approximate and parallel Hartree–Fock and hybrid DFT calculations. A 'chain-of-spheres' algorithm for the Hartree–Fock exchange. *Chem. Phys.* **2009**, *365* (1–3), 98–109.

(18) Vey, J. L.; Yang, J.; Li, M.; Broderick, W. E.; Broderick, J. B.; Drennan, C. L. Structural basis for glycyl radical formation by pyruvate-formate lyase activating enzyme. *Proc. Natl. Acad. U.S.A.* **2008**, *105* (42), 16137–16141.

(19) Bruice, T. C.; Benkovic, S. J. Chemical Basis for Enzyme Catalysis. *Biochemistry* **2000**, *39* (21), 6267–6274.

(20) Rohac, R.; Martin, L.; Liu, L.; Basu, D.; Tao, L.; Britt, R. D.; Rauchfuss, T. B.; Nicolet, Y. Crystal Structure of the [FeFe]-Hydrogenase Maturase HydE Bound to Complex-B. *J. Am. Chem. Soc.* **2021**, *143* (22), 8499–8508.

(21) Cosper, N. J.; Booker, S. J.; Ruzicka, F.; Frey, P. A.; Scott, R. A. Direct FeS Cluster Involvement in Generation of a Radical in Lysine 2,3-Aminomutase. *Biochemistry* **2000**, *39* (51), 15668–15673.

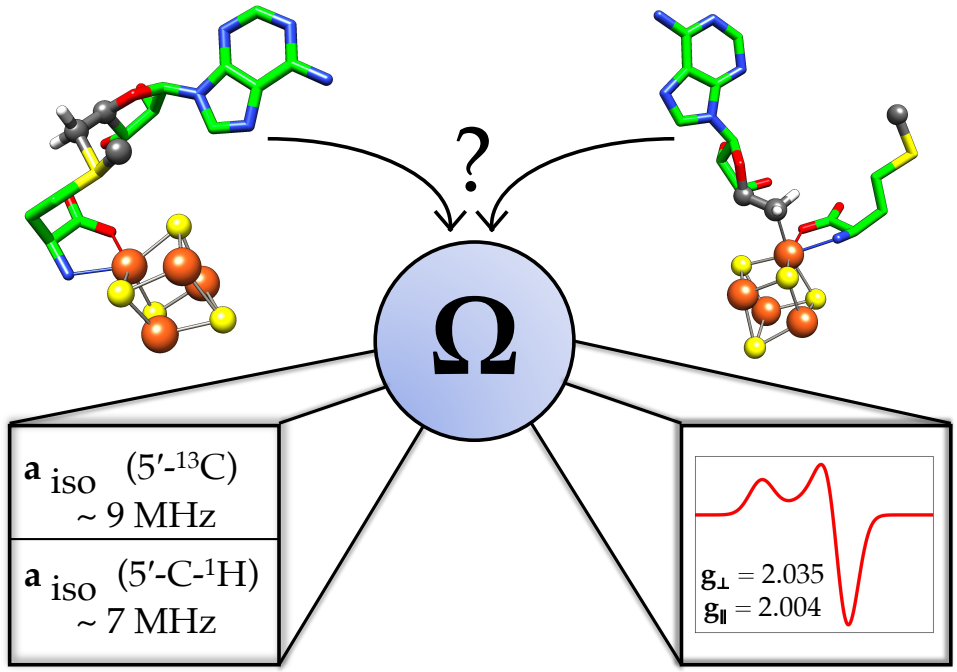

TOC Graphic